Geochemistry Geophysics Geosystems G3

Article
Volume 11, Number 7
28 July 2010
Q07014, doi:10.1029/2010GC003066
ISSN: 1525-2027

Published by AGU and the Geochemical Society

Click Here for Full Article

Sahara Slide: Age, initiation, and processes of a giant submarine slide

Aggeliki Georgiopoulou
National Oceanography Centre, Southampton, European Way, Southampton SO14 3ZH, UK

Now at School of Geological Sciences, University College Dublin, Belfield Campus, UCD Science Centre (West), Dublin 4, Ireland (aggie.georg@ucd.ie)

Douglas G. Masson and Russell B. Wynn
National Oceanography Centre, Southampton, European Way, Southampton SO14 3ZH, UK

Sebastian Krastel
Leibniz Institute of Marine Sciences at University of Kiel (IFM-GEOMAR), Wischhofstrasse 1-3, Gebäude 4, D-24148 Kiel, Germany

[1] The Sahara Slide is a giant submarine landslide on the northwest African continental margin. The landslide is located on the open continental slope offshore arid Western Sahara, with a headwall at a water depth of ~2000 m. High primary productivity in surface waters drives accumulation of thick fine-grained pelagic/hemipelagic sediment sequences in the slide source area. Rare but large-scale slope failures, such as the Sahara Slide that remobilized approximately 600 km^3 of sediment, are characteristic of this sedimentological setting. Seismic profiles collected from the slide scar reveal a stepped profile with two 100 m high headwalls, suggesting that the slide occurred retrogressively as a slab-type failure. Sediment cores recovered from the slide deposit provide new insights into the process by which the slide eroded and entrained a volcaniclastic sand layer. When this layer was entrained at the base of the slide it became fluidized and resulted in low apparent friction, facilitating the exceptionally long runout of ~900 km. The slide location appears to be controlled by the buried headwall of an older slope failure, and we suggest that the cause of the slide relates to differential sedimentation rates and compaction across these scarps, leading to local increases of pore pressure. Sediment cores yield a date of 50–60 ka for the main slide event, a period of global sea level rise which may have contributed to pore pressure buildup. The link with sea level rising is consistent with other submarine landslides on this margin, drawing attention to this potential hazard during global warming.

Components: 11,000 words, 13 figures, 1 table.

Keywords: Sahara Slide; northwest Africa; turbidite; debris flow; slope instability; tsunami.

Index Terms: 3070 Marine Geology and Geophysics: Submarine landslides; 3022 Marine Geology and Geophysics: Marine sediments: processes and transport; 3045 Marine Geology and Geophysics: Seafloor morphology, geology, and geophysics.

Received 25 January 2010; **Revised** 7 May 2010; **Accepted** 19 May 2010; **Published** 28 July 2010.

Georgiopoulou, A., D. G. Masson, R. B. Wynn, and S. Krastel (2010), Sahara Slide: Age, initiation, and processes of a giant submarine slide, *Geochem. Geophys. Geosyst.*, *11*, Q07014, doi:10.1029/2010GC003066.

Copyright 2010 by the American Geophysical Union

1. Introduction

[2] Passive continental margins accumulate large volumes of sediment, often leading to slope instability and submarine mass movement [*McAdoo et al.*, 2000; *Huehnerbach et al.*, 2004; *Masson et al.*, 2009]. The largest submarine landslides are often associated with high sediment input from river deltas or glacial systems [e.g., *Weaver et al.*, 2000; *Bryn et al.*, 2003; *Loncke et al.*, 2009], but large submarine landslides are also surprisingly common on passive margins characterized by lower sediment input [*McAdoo et al.*, 2000; *Huehnerbach et al.*, 2004; *Henrich et al.*, 2008; *Twichell et al.*, 2009]. The preconditioning factors and triggering mechanisms that generate large submarine slides offshore presently arid regions like northwest Africa, where sediment input is low, remain poorly understood [*Weaver et al.*, 2000; *Wien et al.*, 2007]. The northwest African margin is passive and large earthquakes are rare although moderate magnitude earthquakes have been recorded and are attributed to old zones of weakness created during the opening of the Atlantic Ocean [*Hayes and Rabinowitz*, 1975].

[3] Continental slope gradients range from 1 to 6°, while the continental rise displays gradients of <1° [*Masson et al.*, 1992]. The northwest African margin, particularly the area off Western Sahara, receives very little fluvial input [*Summerhayes et al.*, 1976; *Weaver et al.*, 2000]. Canyons are largely absent from this part of the margin, and the existing canyons do not generally reach upslope to the shelf edge and rarely extend downslope beyond the slope-rise boundary.

[4] An upwelling system characterizes the northwest African margin between about 15 to 30°N, driven by the Northeast Trade Winds [*Sarnthein et al.*, 1992]. Productivity in the upwelling region has remained active through glacial and interglacial periods, but with overall higher productivity during glacial. The highest productivity however, occurs during deglaciation [*Bertrand et al.*, 1996]. Aeolian input has also been linked with climatic variability with high input during glacial times and maxima occurring during deglaciations due to strengthening of the wind stress [*Moreno et al.*, 2001; *Bozzano et al.*, 2002]. Overall, sedimentation rates on the upper slope are on average around 5 cm/ka, although during the last glacial period they reached 16.5 cm/ka [*Bertrand et al.*, 1996].

2. Previous Studies

[5] The headwall of the Sahara Slide, one of the largest known slides in the world, is located in the northern reaches of the NW African upwelling system, between 24° and 28° N (Figure 1). Only a few studies exist on the Sahara Slide, mainly concentrating on the descriptive characteristics of the slide and the depositional processes [*Embley*, 1976, 1982; *Embley and Jacobi*, 1977; *Simm and Kidd*, 1984; *Gee et al.*, 1999, 2001].

[6] The Sahara Slide was first referred to as the Spanish Saharan Slide [*Embley*, 1976, 1982; *Embley and Jacobi*, 1977]. In more recent literature it is referred to as Saharan Debris Flow [*Masson et al.*, 1993; *Gee et al.*, 1999, 2001]. We now recognize it as a complex landslide comprising elements of slide in a strict sense as well as debris flow. To avoid further nomenclature changes, we will use the term "Sahara Slide" to describe the overall landslide. Here "slide" is used as an abbreviation of "landslide" and carries no implication of a particular process.

[7] *Embley* [1976] mapped and described the scar area of the Sahara Slide off Western Sahara. It was later estimated that 600 km^3 of Neogene sediments was involved in this slide [*Embley and Jacobi*, 1977]. Sediment samples from the continental slope and upper continental rise off Western Sahara yielded an age of 15–16 ka [*Embley*, 1982]. Another younger event in the range of 2–5 ka was also dated [*Embley*, 1982]. The age of the Sahara Slide was later revised by *Gee et al.* [1999] who examined the distal part of the Sahara Slide deposit and estimated it to be circa 60 ka based on dominant coccolith assemblage ratios in hemipelagic sediments immediately below the base of the slide deposit. They also discovered that the slide was bimodal: an upper layer of plastically deformed pelagic and hemipelagic sediments, which they named pelagic debris flow phase that was carried passively on top of a basal volcaniclastic layer, which they named volcaniclastic debris flow phase. They attributed the long runout of the slide to the volcaniclastic basal layer.

[8] *Georgiopoulou et al.* [2007] found that the headwall area has been the site of numerous massive landslides since at least Miocene times, as recorded by multiple buried events. They showed that landsliding has been taking place retrogressively and proposed differential compaction across buried scarps as the main preconditioning factor driving repeated instability. Evidence for further sliding in

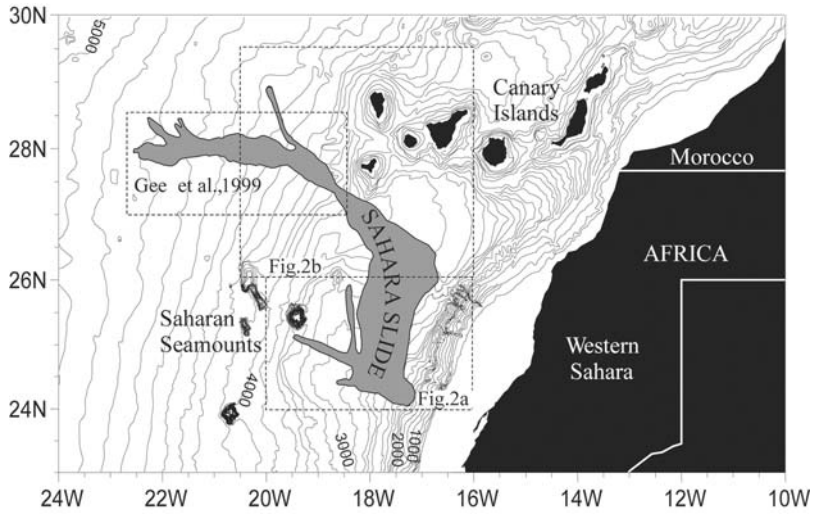

Figure 1. Location of the Sahara Slide on the northwest African margin. The dashed boxes show the areas of investigation for this study as well as the study area of *Gee et al.* [1999]. Bathymetric contours in meters (source: GEBCO).

the headwall area, occurring as recently as the Late Holocene, was presented by *Georgiopoulou et al.* [2009]. They showed that this 1–2 ka old event is related to a linked debrite-turbidite deposit (in the sense of *Haughton et al.* [2003]) found further downslope and a surficial turbidite deposit covering a large area of the northwest African margin. This was thought to have been generated from the debris flow by flow transformation [*Frenz et al.*, 2009; *Georgiopoulou et al.*, 2009]. *Georgiopoulou et al.* [2009] also generated a stratigraphic framework for sediments in the area south of the Canary Islands [*Georgiopoulou et al.*, 2009, Figure 2].

[9] It is timely to revisit the Sahara Slide in the light of new data from the headwall scarps and downslope depositional area. Here we combine new geophysical and sedimentological data from the Sahara Slide in order to constrain the timing of the slide more accurately, its trigger and failure mechanisms, and the resulting flow processes. We also present evidence on the origins of the volcaniclastic basal layer that *Gee et al.* [1999] previously described. Finally, we discuss whether the Sahara Slide could have generated a catastrophic tsunami and draw some conclusions about what drives mass movements on the northwest African margin.

3. Materials and Methods

[10] Data for the study of the Sahara Slide were collected during RV *Meteor* cruises M58/1 and M65/2 and RRS *Charles Darwin* cruise CD126 (Figure 2). This data includes Parasound profiles, one gravity core and nine piston cores (Figure 2). A compilation of 3.5 kHz and Parasound profiles collected during various other surveys complete the geophysical data set.

[11] All cores were logged on Multi Sensor Core Loggers, at BOSCORF (British Ocean Sediment Core Research Facility) in Southampton and at the Geosciences Department of Bremen University, to obtain gamma ray density, magnetic susceptibility and P wave velocity measurements. X radiographs were produced for cores C11, C12 and C13 as their position on the seismic data indicated that they had sampled the margin of the Sahara Slide but visually they appeared not to contain Sahara Slide material. All turbidites in the cores were sampled for grain size analysis and sand fraction mineralogy and the pelagic (background) layers for coccolith assemblages. The latter were combined with the oxygen isotope analysis that already existed for core C12 [*Georgiopoulou et al.*, 2009] to date the Sahara Slide and other gravity flow deposits that are present. The coccolith species identified and counted were *Emiliania huxleyii, Gephyrocapsa muellearae/oceanica, Gephyrocapsa aperta, Gephyrocapsa carribeanica*, and *Pseudoemiliania lacunosa* which are the five dominant species for the past 550 ka [*Weaver and Kuijpers*, 1983]. This methodology is based on the fact that the abundance of different species varies with time and single species become dominant for short time intervals, known as acme zones which follow a consistent pattern in the North Atlantic [*Weaver and Thomson*, 1993].

[12] The characteristics of the cores that were used to establish their chronostratigraphy were as

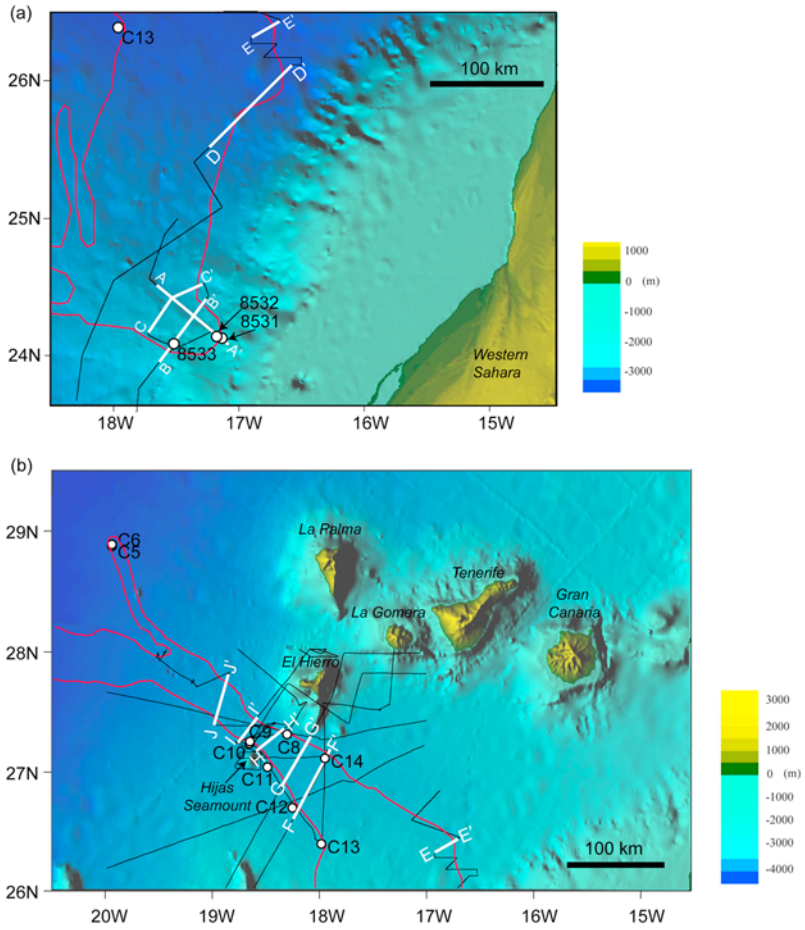

Figure 2. Shaded 3-D bathymetry maps showing (a) the data set distribution at the headwall and (b) the central deposit of the Sahara Slide (red line). All seismic data (3.5 kHz, Parasound, and air gun) are shown in black solid lines. Core locations are indicated with white circles. White solid lines indicate the positions of illustrated sections in Figures 4–6 and 9 (source: GEBCO).

follows: (1) the 2/3 Oxygen Isotope Stage (OIS) boundary, which is marked by a distinct color change in the sedimentary succession (brown foraminifera-free glacial clay to beige foraminifera-rich interglacial marl) as well as a sharp decrease down core in the magnetic susceptibility (this boundary is also confirmed by the oxygen isotope curve (Figure 3)); (2) the OIS 4/5 boundary marked by the last appearance of *Gephyrocapsa aperta* and the percentage of *Emiliania huxleyi* <60%; (3) a peak in the ratio of *Gephyrocapsa muellerae* during substage 5.2; (4) a peak of *Gephyrocapsa aperta* between stages 5.4 and 5.5, and another in substage 6.4; and (5) dominance of *Gephyrocapsa aperta* at the end of OIS 7 and beginning of OIS 6 (Figure 3).

[13] A multiproxy approach was taken to core correlation including analysis of turbidite thickness, sand fraction composition, mud color, magnetic susceptibility, relative position of layers within the core, and coccolith-based dating of background hemipelagic/pelagic sediments [*Wynn et al.*, 2002].

4. Results

4.1. Sahara Slide Morphology

[14] The Parasound profile A–A′ perpendicular to the slope shows an impressive 100 m high headwall scarp that abruptly cuts a continental slope of 1.5° gradient at 1900 m water depth (Figure 4). The seafloor upslope from this scarp appears smooth, with stratified sediments in the subsurface. Below the scarp a thin sheet of blocky slide debris covers the seafloor for some 60 km downslope, where another slide scarp, also 100 m high, steps the seafloor down toward the northwest (Figure 4b). The slope gradient between the two headwalls

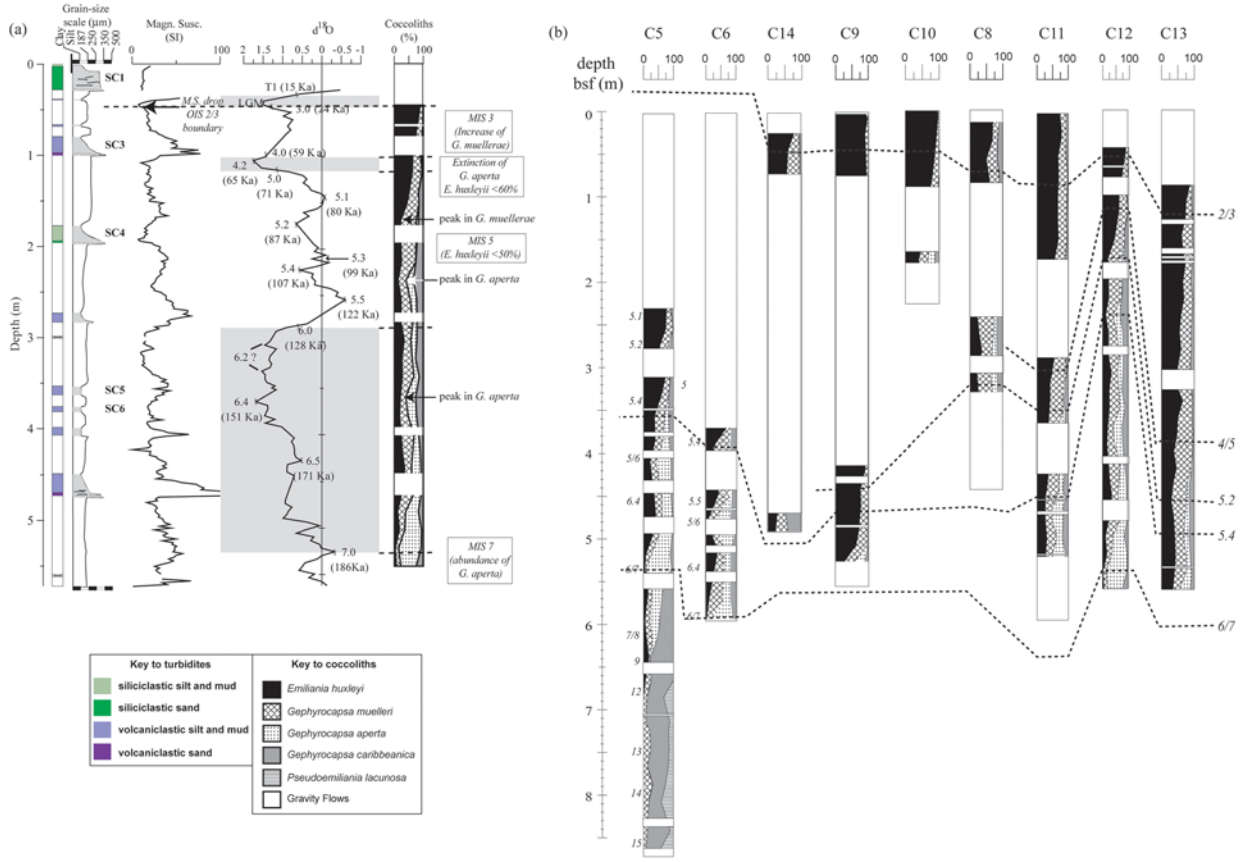

Figure 3. (a) Graphic log, interpretation, magnetic susceptibility, and dating of core C12 using oxygen isotope stratigraphy and dominant coccolith species counts (modified from *Georgiopoulou et al.* [2009]). Note the abrupt decrease in magnetic susceptibility across OIS boundary 2/3. (b) Dominant coccolith species counts in all piston cores used to establish their stratigraphy. Key observations are that *E. huxleyii* is less than 60% with last appearance of *G. aperta* at OIS boundary 4/5; there is a peak in *G. muellerae* during substage 5.2; there are peaks in *G. aperta* between substages 5.4 and 5.5 and during substage 6.4; and finally, *G. aperta* is dominant at the end of OIS 7. The dashed lines show tie points identified across the piston cores.

ranges from 0.4°–1.3° (Figure 4a). The steepest part of the slope lies directly below the upper headwall, where it also appears completely stripped of slide debris (Figure 4d). The slide debris between the two scarps has an average thickness of 10 m and thickens immediately below slope breaks, which are believed to be internal scarps up to 25 m high (Figure 4c) [*Georgiopoulou et al.*, 2009]. At least three internal scarps can be identified on profile A–A′; these give the headwall area a stepped profile consisting of a series of discrete glide planes at different stratigraphic levels offset by discrete scarps with >10° inclination. The two 100 m high headwalls and a series of sidewalls

Figure 4. (a) Parasound dip profile A–A′ along the slide axis showing the upper and lower headwalls (~100 m high each). Spilling over (b) the lower headwall, (c) a thin layer of slide debris of a Late Holocene headwall reactivation can be seen that thickens immediately downslope of internal scarps. (d) Locations of cores GeoB8531 and GeoB8532 of *Georgiopoulou et al.* [2009] are also shown (modified from *Georgiopoulou et al.* [2009]). (e) Parasound profile B–B′ crossing the proximal part of the slide showing the complexity of headwall scarps and division of the scar area into outer and inner scar areas. Multiple scarps can be seen at the southwest boundary of the slide, but there is only one ~75 m high scarp at the northeast boundary. The location of core GeoB8533, which penetrated an intact slide block beneath a strong reflector, is also shown. (f) Parasound profile C–C′ across the proximal part of the slide, parallel to profile B–B′ but a few kilometers to the northwest. Note the decrease in height of the southwest and northeast scarps of the inner scar area. The northeast scarp truncates stratified channel levee sediments. For location of profiles, see Figure 2.

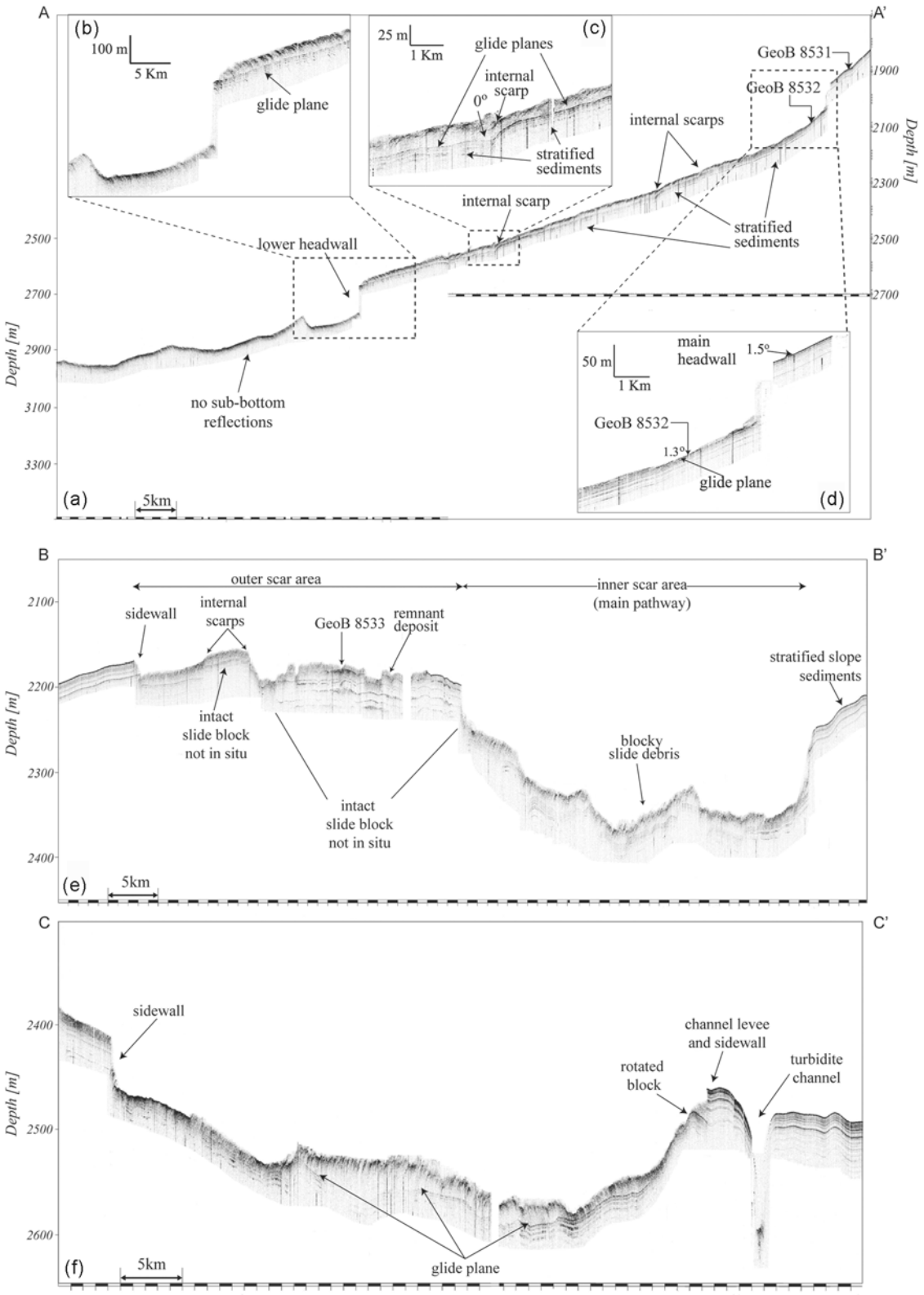
A
A'
(b)
100 m
5 Km
glide plane
(c)
25 m
1 Km
glide planes
internal scarp
0°
stratified sediments
GeoB 8531
GeoB 8532
internal scarps
internal scarp
stratified sediments
lower headwall
no sub-bottom reflections
Depth [m]
2500
2700
2900
3100
3300
1900
2100
2300
2500
2700
50 m
1 Km
main headwall
1.5°
GeoB 8532
1.3°
glide plane
(d)
(a)
5km
B
B'
outer scar area
inner scar area (main pathway)
sidewall
internal scarps
GeoB 8533
remnant deposit
stratified slope sediments
intact slide block not in situ
blocky slide debris
intact slide block not in situ
2100
2200
2300
2400
(e)
5km
C
C'
sidewall
channel levee and sidewall
rotated block
turbidite channel
2400
2500
2600
(f)
5km
glide plane

Figure 4

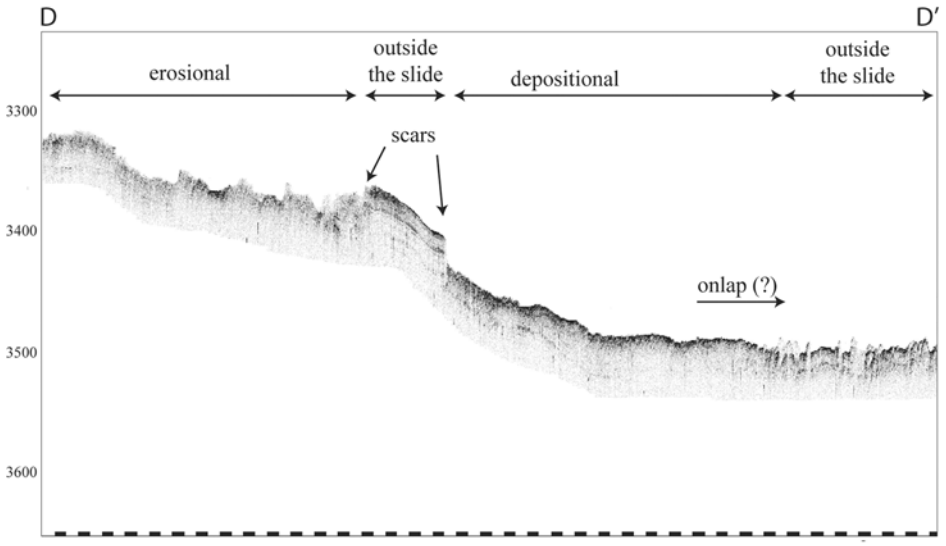

Figure 5. Parasound profile D–D′ showing a change in the morphology of the Sahara Slide from being erosional and forming scarps on the seafloor to depositional with an onlap relationship to the seafloor. For location, see Figure 2.

shape the scar area into an outer scar area and an inner scar area (the inner trough of *Embley* [1980]).

[15] The south and southwestern boundaries of the Sahara Slide headwall region are formed by a series of small scarps, 25–35 m high (Figure 4e). This "outer scar area" has undergone erosion and removal of sediment but has not been deeply excavated. A thin drape of high acoustic amplitudes, interpreted as blocky slide debris, covers the seafloor (Figure 4e). This area of shallow sliding passes northward into a 35 km wide deeper trough ("inner scar area" in Figures 4e and 4f), which is bordered to the southwest by a 50 m high scarp and to the northeast by a 75 m high scarp, with gradients of 4–8°. The northeast boundary of this trough is also the northeast boundary of the slide. The floor of the inner scar area has variable relief. Several weak discontinuous reflectors can be seen below the slide deposit, and the average thickness of the deposit is 20 m.

[16] The inner scar area is the main conduit, where the slide is channelized within erosional scarps, as suggested by the reflectors truncated by those scarps. At least two blocks of nearly intact slope sediments can be identified in the outer scar area with a thin cover of debris (Figure 4e). These are interpreted to be remobilized blocks of slope sediments from further upslope, as the internal reflectors have an irregular appearance in comparison with parallel-bedded in situ sediments.

[17] Further downslope, toward the northwest, the inner scar area widens by more than 10 km. The deposit within it is still generally about 20 m thick, but the sidewalls have become steeper (Figure 4f). The southwest scarp is 50 m high and has a 10° gradient, while the northeast scarp is about 30 m high with a 15° gradient. The scarp bounding the slide to the east decreases in height toward the north until it disappears, at which point an onlapping relationship develops between the slide and the contemporaneous seafloor (Figure 5). This change can be seen at 26°N. The reason for this may be related to local topography and decreasing gradient that affect the dynamics of the flow.

[18] A series of strike profiles across the middle part of the Sahara Slide show how the character of the deposit changes through the topographic constriction between El Hierro Island and Hijas Seamount (Figure 6). Slide deposits pinch out against the lower slopes of both these major topographic features, and also pinch out against small bathymetric highs within this area of rough topography (Figure 6, profile G–G′). Where the topographic gap is narrowest, the Sahara Slide appears to onlap a local slide from the slope of the Hijas Seamount (Figure 6, profile H–H′). Deposit thickness decreases from 25 m immediately upslope of the topographic gap to 15 m within it (Figure 6, profiles H–H′ and I–I′)). This is presumably a response to the increase in seafloor gradient [*Gee et al.*, 2001] that occurs in the area of the gap.

4.2. Seismic Stratigraphy

[19] Seismic reflectors parallel to the slope can be identified below slide deposits in some areas (Figure 4). These reflectors are almost continuous, although at locations where the slide deposit becomes thicker their apparent acoustic impedance is low due to the loss of signal as it passes through the thicker slide deposit. Below the lower headwall, the slide deposit thickness increases to >30 m. The acoustic character is transparent with no internal reflectors and the base of the slide cannot be seen as the acoustic signal appears to be entirely absorbed by the slide material (Figure 4).

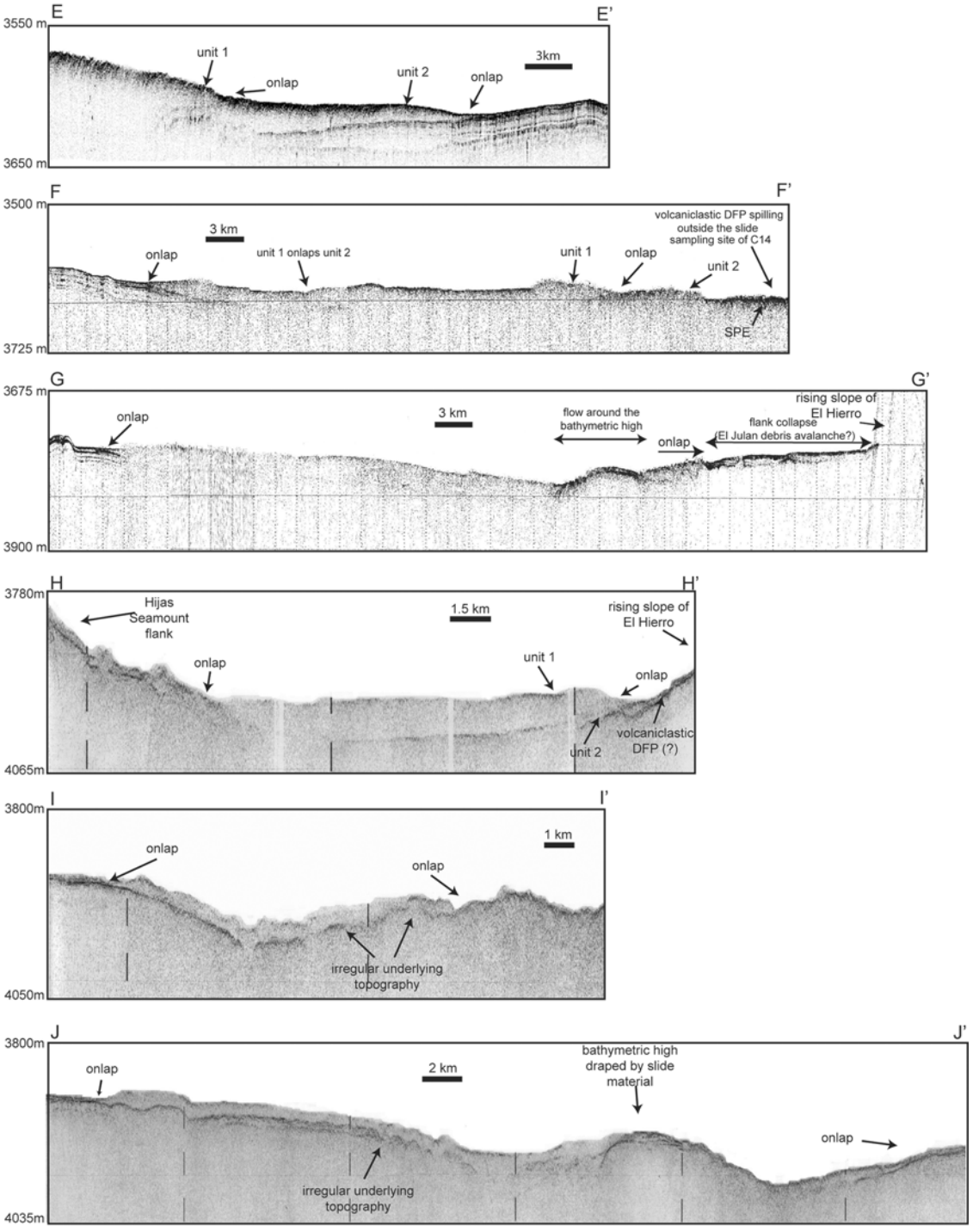

Figure 6

[20] Downslope, the 3.5 kHz and Parasound profiles demonstrate the lenticular shape of the slide in cross section and the onlap relationship with preexisting seafloor sediments (Figure 6). Slide deposits are acoustically transparent and the seafloor within the slide area generally appears as a low-amplitude reflector compared to the seafloor outside the slide. However, in places it displays higher amplitude, which probably reflects the presence of more coherent blocks within the slide mass. In most of the profiles the northeast boundary of the slide appears to comprise two stacked acoustically transparent units (Figure 6, profiles E–E′, F–F′, and H–H′), which display onlapping relationships with each other and the contemporaneous seafloor. The deeper unit (unit 2) has the wider areal extent. The younger unit (unit 1) always onlaps unit 2, and for this reason it is believed that unit 2 is the one that has been sampled by piston cores that were aiming for the slide margins. Unit 2 thins rapidly at its northeast limit and the reflector becomes stronger and prolonged, with a "fuzzy" signature. *Gee et al.* [1999] call this type of reflector "strongly prolonged echoes," which they interpret as the reflection character of the volcaniclastic DFP. The southwest boundary on these profiles also shows the presence of units 1 and 2, with unit 2 onlapping the seafloor.

4.3. Sedimentology of the Sahara Slide

[21] A gravity core (GeoB 8533) was taken near the southern boundary of the slide scar from the outer scar area (Figures 2 and 4). The cored sequence that most likely forms part of the recent headwall collapse [*Georgiopoulou et al.*, 2009], consists of highly deformed "background" slope sediments that include clays, silty clays, sands and oozes (Figure 7). The top of a slide deposit is at ~10 cm depth below the seafloor, with hemipelagic olive-green mud deposited above it. The density log confirms this boundary with a sharp drop in density up core (Figure 7). Density peaks (two of them >2000 gr/cc) occur in the core between 395 and 500 cm. One of these peaks, at 467 cm bsf (44 cm in section 7) (Figure 7), coincides with a lithological boundary between clay and sand. The other peaks, however, are consistently found a few centimeters above such lithological boundaries. At 512 cm bsf there is sharp drop in density down core. This boundary is characterized by shear structures (Figure 7c).

[22] Nine piston cores, collected from the margins of the Sahara Slide in the area south of the Canary Islands, consist of pelagic/hemipelagic "background" sediments, including clays, marls and oozes, interrupted by gravity flow deposits (i.e., turbidites and slide deposits). Six of them (C5, C6, C8, C9, C10, and C14) retrieved Sahara Slide material and one (C13) fell just outside the slide boundary. Cores C11 and C12 were more enigmatic as they do not contain Sahara Slide sediments but seismic profiles suggest that the margin of the slide should have been sampled. X-radiographs of sections of these cores showed slight disturbance of the in situ sediments such as shear boundaries and distorted bioturbation (Figure 8).

[23] Cores C5, C6, C14, and C9 contain Sahara Slide sediments in thicknesses varying from 1.2 to 3.7 m. They penetrated both pelagic debris flow phase (pelagic DFP) and volcaniclastic debris flow phase (volcaniclastic DFP) of *Gee et al.* [1999]. Note that the term "phase" refers to the differing sedimentological character of the two layers of the debris flow, which are believed to have been emplaced simultaneously. The pelagic DFP consists of contorted sediments including pelagic/hemipelagic oozes, clays and marls and interbedded turbidites (Figure 9); this unit appears either as folded sedi-

Figure 6. Profiles illustrating the changing character of the Sahara Slide through the constricted area between the island of El Hierro and Hijas seamount. Parasound profile E–E′ across the eastern boundary of the Sahara Slide east of the constriction shows at least two units of slide material stacked on top of each other. The material shows the transparent seismic character typical of mass flow deposits. Note the difference of acoustic impedance of the seafloor reflector on unit 1 (hyperbolae and not very strong) compared to unit 2 (higher acoustic impedance and no hyperbolae). The 3.5 kHz profile F–F′ across the width of the Sahara Slide shows two slide units on the southwest and northeast boundaries of the Sahara Slide. Also indicated is an area of strongly prolonged echoes (SPE [*Gee et al.*, 1999]), the reflection character of the volcaniclastic DFP. The 3.5 kHz profile G–G′ across the width of the Sahara Slide demonstrates the capacity of the Sahara Slide to infill local topography and flow around topographic highs. The 3.5 kHz profile H–H′ across the width of the Sahara Slide illustrates the lenticular geometry of the slide deposit and its constriction by the Hijas Seamount to the southwest. Two units of material can be seen onlapping the northeast boundary. The 3.5 kHz profile I–I′ at the narrowest point of the Sahara Slide demonstrates the irregular topography of the seafloor in this area and the reduced thickness of the deposit. The 3.5 kHz profile J–J′ is located west of the topographic constriction, where the Sahara Slide widens and remains thin. Its high mobility is expressed by its capacity to flow around topographic highs. Locations of profiles are indicated in Figure 2.

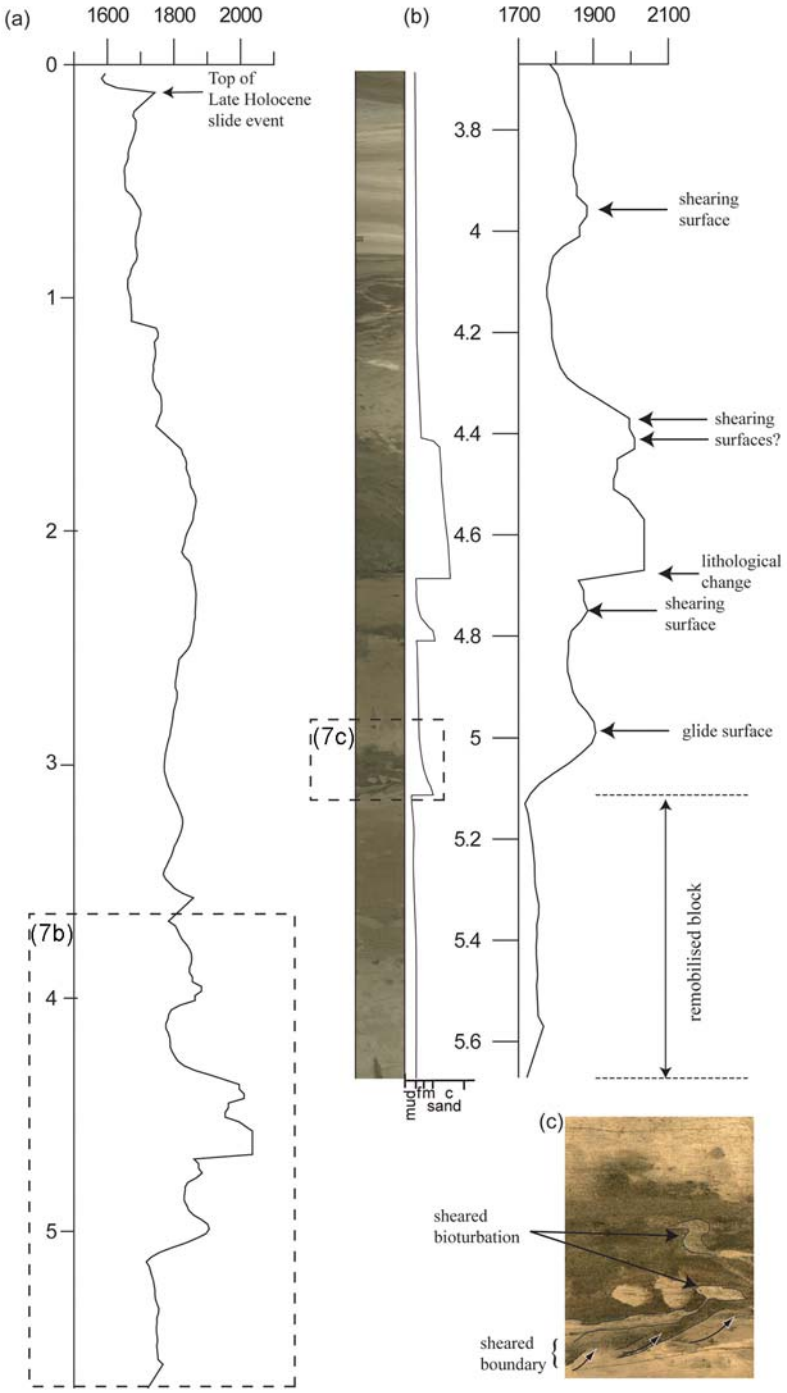

Figure 7. (a) Density log of the top 565 cm of core GeoB 8533. The top of the slide, marked with arrow in Figure 7a, is expressed as a peak in the density response that drops off upward demonstrating the difference in the properties of the sediments deposited on top of the slide. (b) The log reveals three shear surfaces where the density peaks at about 2000 gr/cc and then drops off. Note that they occur in the fine-grained sediments directly above sandy layers. (c) The strong reflector in Figure 4e correlates with a sand layer sampled in the core where some shearing appears to have occurred (arrows in Figure 7c). See Figures 2 and 4 for core location.

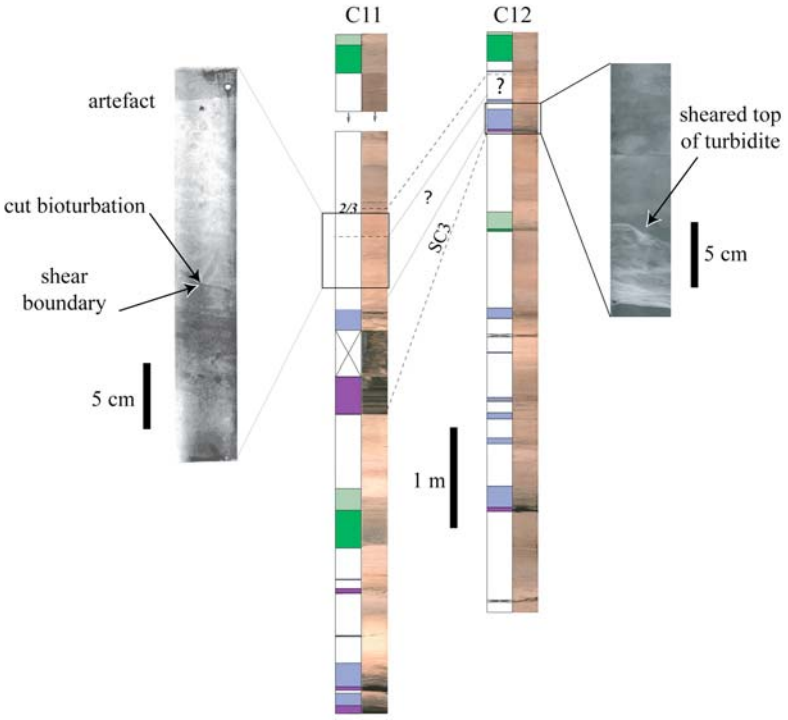

Figure 8. Photograph and interpretation of cores C11 and C12. The X-radiographs of sections of the cores immediately above turbidite SC3 show shear boundaries interrupting bioturbation in C11 and disturbing the lamination at the top of turbidite SC3 in C12. The X-radiographs confirm disturbance of the seafloor sediments at the site of cores C11 and C12, even though no slide sediments were sampled.

ment packages with shear boundaries or as alternating thin layers of slope sediments and reworked volcaniclastic turbidites. In some cases extensive shearing has thinned the sediment layers, largely destroying any original structure. The volcaniclastic DFP consists of a very stiff mixture of poorly sorted, angular volcanic sand in a fine-grained nannofossil clay grade matrix. In all four cores that penetrated both DFP, the volcaniclastic DFP is seen to underlie the pelagic DFP, but it also occurs as discrete layers within the pelagic DFP or forms a coating on clasts (Figure 9).

[24] Core C8 contains what appears to be a folded clast. The base of this clast, which is a layer of beige marl, lies above a layer of structureless, poorly sorted volcaniclastic sand (Figure 10). The contact is a transitional erosive boundary, where the marl and the volcaniclastic sand have apparently been partially mixed. Core C10 has a similar boundary at about 140–150 cm depth.

[25] Samples were taken for grain size analysis from all cores that contain the volcaniclastic DFP and also from core C8 (Figure 10). The volcaniclastic DFP has remarkably consistent grain size spectra in all cores, characterized by three peaks (Figures 10f–10k [see also *Gee et al.*, 1999]). The spectra of the three samples from core C8 were taken from (1) pelagic/hemipelagic background sediment, (2) the transition zone between the pelagic sediment and the volcaniclastic sand, and (3) from pure volcaniclastic sand (Figure 10). Depending on lithology, up to three characteristic grain size peaks occur: at 3–4.5 microns, that is produced by coccoliths, 20–70 microns, produced by foraminifera and 350–400 microns produced by medium volcaniclastic sand (Figure 10).

[26] Grain size spectra of varied mixtures of the end-member pelagic/hemipelagic and volcaniclastic lithologies (Figures 10a and 10c) were then modeled (Figures 10d and 10e) to examine whether the volcaniclastic DFP could be produced by mixing of the pelagic DFP with the volcaniclastic sand. A good match for the sample from the transition zone (Figure 10b) was produced by mixing approximately equal mixtures of spectra in Figures 10a and 10c (Figure 10d). The slightly lower grain size of the main peak in the measured sample (z′ in Figure 10b), compared with the model, is a result of only the upper (finer) part of the graded volcaniclastic turbidite being included in the natural

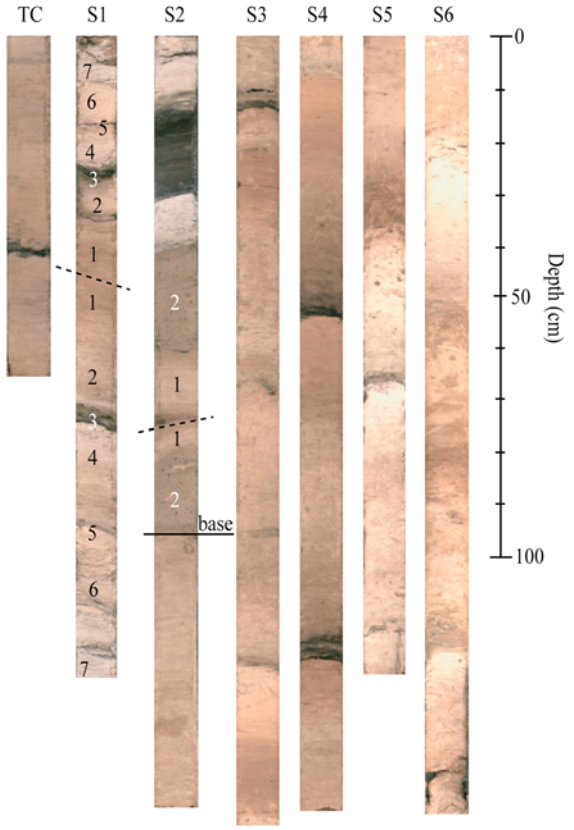

Figure 9. Photograph of core C5. TC is the trigger core, S1 the top section of the core, and S6 is the bottom section. In sections 1 and 2 the numbered sediment units indicate sequences repeated around fold axes (dashed lines). Solid black line indicates the base of the slide. The layers marked with the number *2* are volcaniclastic DFP. The rest of the core consists of in situ clays, marls, and oozes, punctuated by volcaniclastic turbidite deposits (dark gray/black sediment). For core location, see Figure 2.

mixture, whereas the modeled mixture is based on the main coarser part of the turbidite.

[27] The three characteristic peaks of volcaniclastic DFP spectrum can be matched by mixing the pelagic (Figure 10a) and volcaniclastic spectra (Figure 10c), but with pelagic sediment being the dominant component. Our models suggest that the volcaniclastic DFP consists mainly of pelagic sediment (about 90%) with only a minor proportion (10%) of volcaniclastic sand.

4.4. Core Correlation and Interpretation

[28] Core GeoB 8533, collected near the sidewall of the Sahara Slide is interpreted to have sampled only material from the Late Holocene headwall collapse similar to the cores described by *Georgiopoulou et al.* [2009]. High density peaks in this core may reflect shearing boundaries within the slide material as they do not coincide with lithological boundaries, apart from one. Instead they consistently appear within the fine grained pelagic sediments a few centimeters above the sand-clay boundaries (Figure 7). The sheared boundary at 512 cm that coincides with a sharp change in density we interpret to reflect a glide surface on a remobilized block.

[29] An average hemipelagic sedimentation rate of 1.9 ± 0.15 cm/1000 yrs was calculated from core C12. This does not take into account potential erosion of seafloor sediments by the Sahara Slide and turbidity currents. True hemipelagic thicknesses per oxygen isotope stage are difficult to determine in the absence of a core without possible erosional events.

[30] The core correlation panel (Figure 11) is arranged to show the transition from undisturbed seafloor (not affected by the Sahara Slide, e.g., C13) to disturbed seafloor (affected or covered by the Sahara Slide, e.g., C5). The data set can therefore be treated as a cross section of the seafloor before, during and after passage of the slide. Cores can be categorized into three groups based on the amount of disturbance of the seafloor at the time of slide deposition. Hence there are (1) cores that contain slide material with typical mixed and contorted sediments, (2) cores which illustrate the mixing process that produces the basal volcaniclastic debris flow phase, and (3) cores that show very little disturbance of the seafloor by the passage of the slide. In addition, one core (C13) sampled undisturbed seafloor outside the slide boundary.

[31] Cores C10 and C8 are interpreted to have "captured" the mixing process that produces the volcaniclastic DFP. The deformation patterns seen in the X-radiographs of cores C11 and C12 are interpreted to have been generated by the stresses imposed on the seafloor by slide emplacement in the immediately adjacent area.

5. Discussion

5.1. Timing of the Sahara Slide

[32] The core correlation panel shows the stratigraphic position of the Sahara Slide in relation to other mass wasting events and in situ background sediments (Figure 11). The Sahara Slide is con-

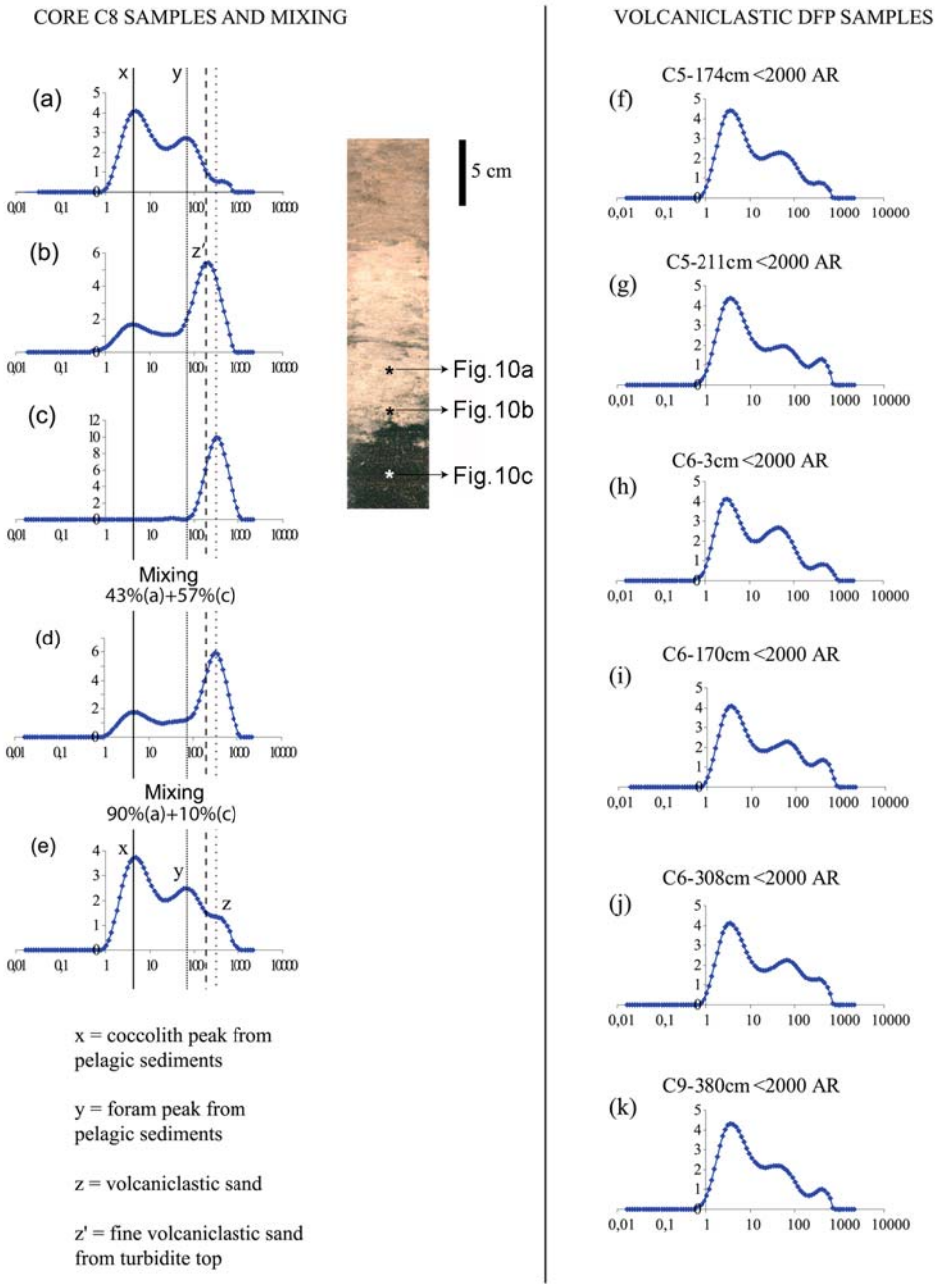

Figure 10. Grain size data from the base of the slide in core C8. Grain size analyses were performed on sediment below 2000 microns using a Malvern Mastersizer 2000. (a–c) The grain size spectra of three samples (indicated with stars on core photograph). The sample in Figure 10a is pure local hemipelagic sediment, and the sample in Figure 10c is pure volcaniclastic turbidite. The sample in Figure 10b is from the mixing zone between the samples in Figures 10a and 10c, where it is inferred that the volcaniclastic turbidite has been partially entrained by passage of the Sahara Slide. (d) A modeled spectrum created by mixing 43% of the sample in Figure 10a with 57% of the sample in Figure 10c. This spectrum is remarkably similar to the spectrum in Figure 10b. (e) Produced by mixing approximately 90% of the sample in Figure 10a with 10% of the sample in Figure 10c. This clearly resembles (f–k) the grain size spectra obtained from numerous volcaniclastic DFP samples. Peak x is dominated by coccoliths, y represents foraminifera, and z and z′ represent volcaniclastic turbidite sand.

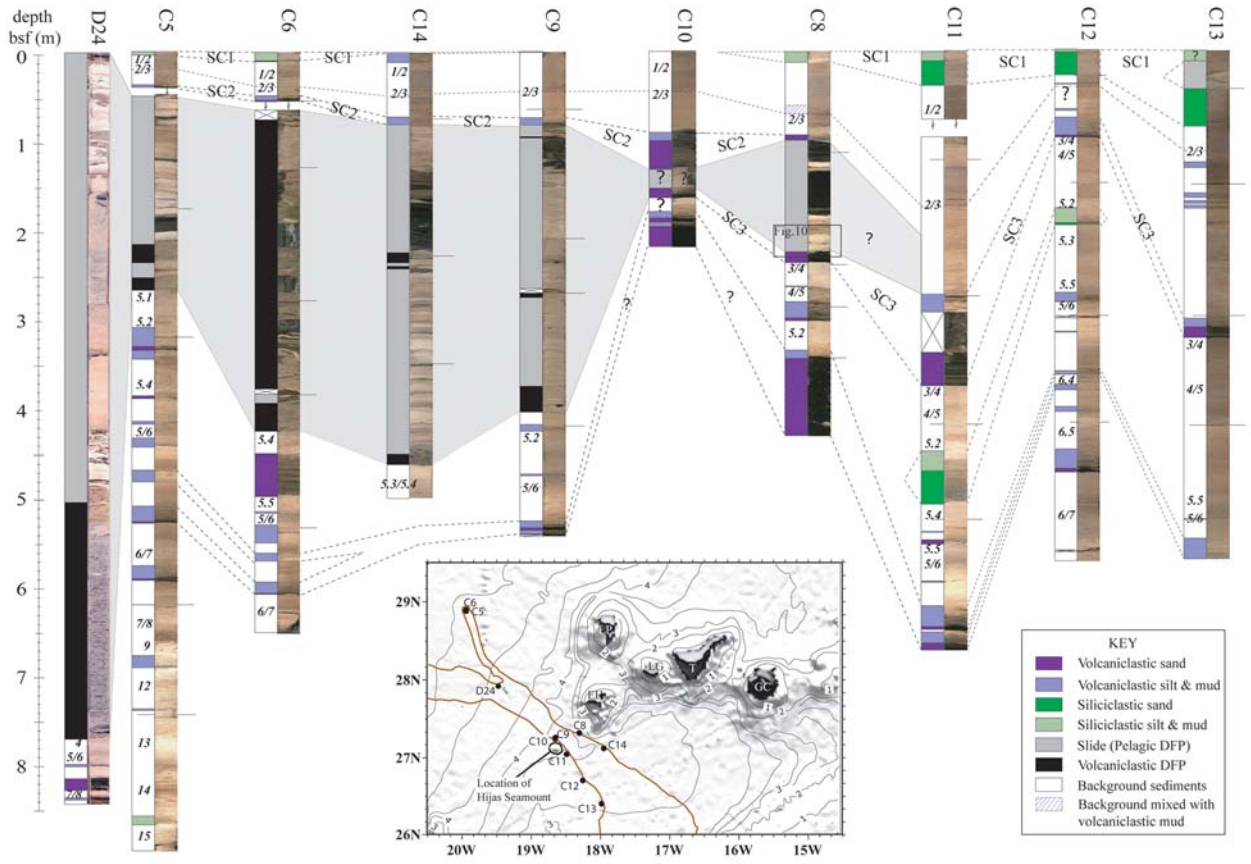

Figure 11. Correlation panel of CD126 piston cores C5–13 and D24 from *Gee et al.* [1999] and interpretation columns with oxygen isotope stages in italics. Cores are arranged in a manner that represents a cross section (from right to left) of the seafloor in the following sequence: seafloor sediments (1) unaffected by the slide, (2) disturbed by the passage of the slide, and (3) eroded by the slide. This core arrangement demonstrates the different character of the Sahara Slide across its margins and the process of formation of the volcaniclastic DFP (see section 4.4 for details). The dashed lines represent correlation lines connecting turbidite deposits (key correlation levels SC1, SC2, and SC3 are labeled) across the cores, and the gray shaded area indicates the Sahara Slide deposit. Cores C11 and C12 do not contain slide deposits but do appear to contain disturbed hemipelagic sediments that formed the seafloor at the time of emplacement of the Sahara Slide. Inset map shows core locations and the margins of the Sahara Slide in this area (brown line).

fined between volcaniclastic turbidites SC2 and SC3 in cores C8, C10, C11, and C12. In C5, C6, C9 and C14, turbidite SC2 occurs directly on top of slide deposits, but turbidite SC3 is not present beneath the slide. Where turbidite SC3 is absent (because of its incorporation into the volcaniclastic DFP), hiatuses due to erosion are observed, the length of which vary between cores.

[33] Investigations of assemblages of the five dominant coccolith species in pelagic/hemipelagic layers above and below turbidite SC3 show that this turbidite was emplaced during the transition from glacial stage 4 to interglacial stage 3, suggesting it was emplaced at 60 ka. Correspondingly, OIS 1–3 are always present above turbidite SC2. In C11 and C12 slide deposits are absent, but deformation of the background sediments can be seen directly above turbidite SC3 which we attribute to stresses on the sediments adjacent to the slide related to slide emplacement. Thus these sediments must have already been deposited on top of turbidite SC3 when the Sahara Slide occurred. However, it is not evident where the top of these deformed sediments, which was actually the seafloor at the time of Sahara Slide emplacement, lies. Nonetheless, it can be argued that the Sahara Slide must have taken place after the 3/4 OIS transition from glacial to interglacial in the early part of OIS 3, probably between 50 and 60 ka, which was a period

of sea level rise. Further downslope, the age *Gee et al.* [1999] found was such because the volcaniclastic turbidite deposited at 60 ka got incorporated at the base of the slide. Thus *Gee et al.* [1999] dated the seafloor on which the volcaniclastic turbidite was deposited, rather than the slightly younger Slide.

5.2. Failure Mechanism and Present-Day Stability

[34] Based on seismic profiler data, the Sahara Slide appears to have occurred as a retrogressive slab-type failure in at least two stages. The two discrete onlapping seismic units observed in the depositional area (Figure 6) may relate to the upper and lower slide headwalls (Figure 4). However, the time interval between these two failure stages is unknown.

[35] Even though the gradient of the slope off Western Sahara is very low, retrogressive slides have been reported in such environments before [*Huehnerbach et al.*, 2004]. According to *Georgiopoulou et al.* [2009] the slope sediments at this location are predominantly fine-grained with rare sandy layers (see core GeoB 8533 (Figure 7)). It is likely that inflow of pore fluids expelled from these sandy layers upward into the less permeable clay sediments led to pore pressure buildup. Potential shearing boundaries with density peaks seen directly above sandy layers and shearing structures at the base of a sandy layer were observed in the headwall (Figure 8). It has been suggested that overpressure in low-permeability fine-grained sediments may build up due to inflow from below or due to lack of permeable coarser-grained layers that would promote drainage [*Flemings et al.*, 2008]. Consolidation under burial will cause pressure to increase due to incompressible fluid (water) filling the pore space [*Dutta*, 1984]. In response, fluid will tend to migrate. If the rate of sedimentation is higher than the rate of water drainage, vertical loading is introduced, which in turn causes excess pore pressure to build up in the sediment layer [*Strout and Tjelta*, 2005]. As a result the layer can be weakened, allowing overlying sediments to move over it under the effect of gravity [*Vendeville and Gaullier*, 2003; *Bryn et al.*, 2005; *Kvalstad et al.*, 2005]. When the unloading is sufficient, moderately sensitive, gently inclined sediments are able to generate progressive spreading of shear bands with strain softening causing initiation of the next step and retrogressive sliding [*Kvalstad et al.*, 2005].

[36] The key element for destabilization in this margin is therefore likely to be pore overpressure in the fine-grained slope sediments. The most probable cause is sediment loading in combination with long sediment residence times on the slope. The timing of the Sahara Slide coincides with a deglaciation (transition from OIS 4 to OIS 3) during which productivity was at a maximum, i.e., at the time of sea level rise, due to intensification of the upwelling cell [*Bertrand et al.*, 1996; *Kuhlmann et al.*, 2004].

[37] Free gas, gas hydrates, diapirism and earthquakes are commonly invoked as external triggers for submarine sliding. No evidence for gas was observed on the seismic data [*Georgiopoulou et al.*, 2007] and diapirism is not a feature of this margin thus these are not likely triggers. Earthquakes are rare and related to old zones of weakness [*Hayes and Rabinowitz*, 1975] that are too distant (100s of kilometers away) to be potential triggers, particularly in combination with the gentle slope gradient where the Sahara Slide took place [*ten Brink et al.*, 2009]. Sedimentation rates are not particularly high at present [*Bertrand et al.*, 1996], supporting present-day stability. Nevertheless, given the steepness of the exposed slide headwalls, and failures such as the Late Holocene headwall reactivation [*Georgiopoulou et al.*, 2009] further small-scale instability cannot be ruled out.

5.3. Seafloor Erosion by the Sahara Slide

[38] Seismic data show that the slide had the capacity to exploit channels and flow around small bathymetric highs which suggests that it was highly fluid and mobile, i.e., a debris flow. This is also observed on side scan sonar data in the more distal part west of the Canary Islands where streamlined high-backscatter material surrounds low-backscatter coherent blocks of sediment [*Masson et al.*, 1993]. It has been observed that the flow sustained this character throughout the travel path, even when it was constricted by topography [*Gee et al.*, 2001]. Downslope from the narrow topographic gap the deposit broadens but maintains its low thickness (~15 m); in this area the flow was still capable of flowing around bathymetric highs (Figure 6). Here the underlying topography is irregular, which can either be explained as an original feature of the seafloor or as the result of increased erosional capacity of the flow due to flow constriction and increased seafloor gradient.

[39] The variation in age of sediments beneath the Sahara Slide demonstrates variable depths of ero-

sion. At least four of the cores (C5, C6, C9 and C14) show significant stratigraphic gaps beneath the slide. The biggest gap is found in core C14 that shows a pelagic layer of oxygen isotope substage 5.4 (107 ka) underlying the Sahara Slide; this gap is equivalent to a ~95 cm thick interval of pelagic/hemipelagic sediments, assuming a 1.9 cm/ka average sedimentation rate as derived from core C12. Although cores C5 and C6 were taken from locations only about 1.5 km apart, the gap is smaller in C5 than in C6. This may reflect the diverse character of the slide and the rapid changes that occur within its body even in short distances. On the other hand this discrepancy could be due to the termination of the slide in the vicinity of these cores and the resulting decrease of its energy and erosive capacity.

[40] *Gee et al.* [1999] suggested that >8 m of sediment had been eroded from beneath the central portion of the slide, based on the observation that coccolith species present in the volcaniclastic DFP indicated that it had incorporated sediment that was at least 500 ka in age. The much smaller amounts of erosion observed in the present study may be the result of the position of our cores at the slide margins, where erosion is likely to be minimal. However, it is also possible that the coccolith assemblages observed by *Gee et al.* [1999] reflect incorporation of material from the pelagic DFP (i.e., from the slide scar on the continental slope) into the volcaniclastic DFP, of which the main component is pelagic sediments (Figure 10), rather than deep erosion along the slide pathway. The slide scar on the Western Sahara slope is formed by two 100 m high scarps, which means that as much as 200 m of Late Pliocene and Pleistocene sediments were excavated from the area.

5.4. Transport and Depositional Processes in the Central Slide Area

[41] Many laboratory experiments have attempted to simulate subaqueous slide processes and reconstruct their behavior [*Mohrig et al.*, 1998, 1999; *Harbitz et al.*, 2003; *Toniolo et al.*, 2004]. Some of these propose that hydroplaning takes place and that the flow has little effect on preexisting seafloor sediments, while others suggest strong interaction with the seafloor and extensive remobilization of preexisting deposits by the slide.

[42] The Sahara Slide has an exceptionally long runout distance, but sedimentological and geophysical data show that it was an erosional, albeit highly mobile, slide. We have shown that the volcaniclastic DFP was produced by mixing of pelagic/hemipelagic sediments at the base of the slide with sediments from the substrate, including a volcaniclastic turbidite (or turbidites) that lay on (or just below) the seafloor at the time of slide emplacement (Figure 10 and section 4.3). Therefore hydroplaning cannot have taken place.

[43] Loading of the volcaniclastic turbidite by the pelagic DFP may have fluidized the sand, allowing it to be incorporated into the base of the slide by shearing and mixing processes. Any seawater that was able to infiltrate the base of the flow would only increase the efficiency of this mixing process. The mixing process would also explain the homogeneity that the volcaniclastic DFP exhibits throughout. However, the quantity of water that intruded into the body of the slide (if any) must have been low enough not to cause disintegration of the slide to the degree that it would transform into a turbidity current. Shearing at the bottom of the slide would tend to slow down the flow, but the product of the mixing, i.e., the volcaniclastic DFP, must have been mobile enough and acted as a low-friction layer helping the slide flow for an extended distance [*Gee et al.*, 1999].

[44] As long as elevated pore pressures were maintained the flow remained mobile. High pore pressure would be sustained either because the overlying pelagic debris flow formed an efficient seal, water was continuously forced out of the underlying volcaniclastic sand, and/or the head of the slide remained lifted in order to allow water to intrude at its base. A model of the Sahara Slide from its initiation on the continental slope to its termination 500 km west of the island of El Hierro can now be constructed (Figure 12).

[45] The lack of a turbidite associated with the main Sahara Slide is puzzling, especially as the recent headwall collapse generated an extensive turbidite deposit [*Georgiopoulou et al.*, 2009]. Considering that the two events took place in the same location and involved the same lithologies, the reason for the difference must be related to the failure process. The main Sahara Slide was a slab-type failure on a low-angle slope, and was therefore likely to have been relatively slow moving. Additionally, given the high cohesiveness of the fine-grained headwall sediments, mixing with ambient seawater would have been hindered, preventing disintegration of the moving slide mass. The recent headwall collapse involved the same sediments but occurred on a steeper slope and propagated on a rough terrain created by the main event, possibly promoting

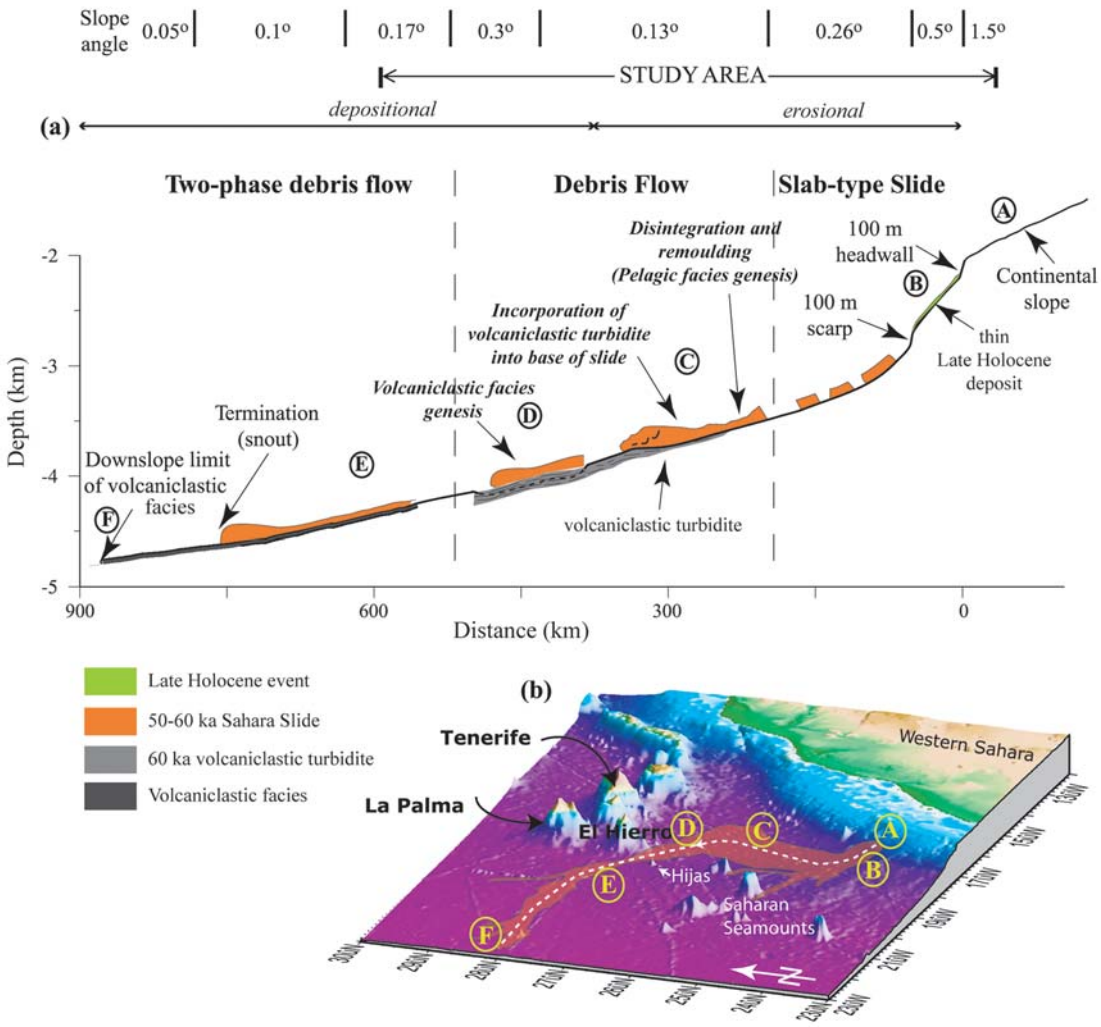

Figure 12. (a) Profile of the Sahara Slide from source to sink. It begins on the continental slope (indicated by A) as a slab-type failure (indicated by B), disintegrates downslope, and transforms into a debris flow (indicated by C). It then incorporates a volcaniclastic sandy turbidite from the substrate south of the Canary Islands to form the volcaniclastic DFP (indicated by D), which gives it a two-phase flow structure (indicated by E). It eventually terminates 500 km west of El Hierro on the continental rise (indicated by F). (b) The profile follows the dashed white line (Sahara Slide shown in orange).

higher velocities and progressive disintegration of the slide mass. As the slide passed over the lower headwall further mixing and water entrainment could have occurred, resulting in flow transformation from debris flow to turbidity current, in the same manner as has been previously suggested for the events of the 1929 Grand Banks earthquake [*Piper et al.*, 1999].

5.5. Could the Sahara Slide Have Generated a Tsunami?

[46] In recent years it has been widely recognized that tsunamis can be generated by submarine landslides [*Bardet et al.*, 2003]. The size of the Sahara Slide suggests that it may have been capable of generating a tsunami. In the absence of direct evidence, we make some informed assumptions about the potential the Sahara Slide had to generate a tsunami based on its dimensions and setting.

[47] The parameters that are significant in determining tsunami characteristics and need to be taken into account are the slide volume, initial slide acceleration and slide velocity, [*Ward*, 2001; *Haugen et al.*, 2005; *Harbitz et al.*, 2006], of which initial acceleration has been argued to be the most important [*Watts et al.*, 2005]. It is difficult to

Table 1. Morphological Characteristics and Ages of Submarine Slides on the NW African Margin[a]

Instability	Total Area (km^2)	Total WDR (m)	Main Scarp (m)	Length × Width (km)	Maximum/ Average Thickness (m)	Volume (km^3)	Source Area/Deposit Toe Slopes	Runout Distances (km)	Age of Main Event (cal yr B.P. or Date)	Main Sources
Sahara Slide	70,000	1900/4900	100	900 × 20–100	?/10	600	1.49°	900	45,000–59,000 latest failure circa 2000	this study and *Embley* [1982]
Canary Debris Flow	40,000	3900/5400	no scarp[b]	600 × 60–90	20/10	400	1°/~0°	600	17,000/13,000	*Masson et al.* [1998]
Cape Blanc Slide	40,000	3575/?	25	? × 175	?	?	0.47°/unknown	>300	155 ka	*Krastel et al.* [2006] and *Wien et al.* [2007]
Mauritania Slide Complex	34,000	800/3500	100	300 × 50–150	?/60	400	1.5°–2.2°/?	300	10,500–10,900	*Antobreh and Krastel* [2006] and *Wien et al.* [2007]
Dakar Slide	?	3500/?	30	?	~100	?	0.8°	?	?	*Krastel et al.* [2006]
Storegga Slide	90,000	130/3850	400	~770 × 115	200/60	≤3000	23°/0.1°	770	8200 latest failure circa 5000	*Haflidason et al.* [2004, 2005]

[a]The Storegga Slide is included for comparison. WDR, water depth range.
[b]The Canary Debris Flow was generated by the El Golfo Debris Avalanche; therefore, there is no scarp.

determine or to estimate the velocity and initial acceleration of the Sahara Slide. However, we believe we can infer that it was a slow slide because the absence of a related turbidite suggests that the slide was not moving sufficiently quickly to generate shear mixing between the slide and the overlying water. Finally it has been numerically shown that large water depths, such as the 1900 m of the Sahara Slide headwall, tend to depress tsunami wave amplitude [*Ward*, 2001].

[48] Another important factor is the mode of failure as retrogressive slides tend to generate smaller tsunamis than similar volume slides that fail as a single block [*Haugen et al.*, 2005] although retrogressive slides are capable of increasing the landward propagating wave [*Harbitz et al.*, 2006]. At least two landslide phases have been mapped, probably resulting in at least two separate waves, each of which would generate a landward propagating wave.

5.6. Slides of the Northwest African Margin

[49] Among the northwest African margin slides the Sahara Slide is clearly the largest in volume, runout distance, as well as affected seafloor area (Table 1). The common characteristics are that they take place in large water depths, more than 1900 m, and on very gentle slopes, less than 2°. This is remarkable considering their size and the volumes of sediment involved, but consistent with previous findings for Atlantic margins slides [*Huehnerbach et al.*, 2004]. The only exception is the Canary Slide, which technically does not originate from the African continental slope but from the Canary Islands and therefore exhibits different characteristics as the lithologies and mode of failure are related to volcanic processes [*Masson et al.*, 1997].

[50] No slides have been mapped on the upper slope, where sediment supply would be expected to be maximum if it was supplied from terrigenous sources. However, sediment buildup on this margin is primarily due to upwelling and increased primary productivity and secondarily to aeolian dust input, while there is no alluvial input [*Krastel et al.*, 2006; *Wien et al.*, 2006]. It is likely then that failure initiation is associated with the position of the upwelling cell and areas of maximum sedimentation rates. Presently, maximum primary productivity is taking place on the slope at water depths between 1000 and 1500 m [*Bertrand et al.*, 1996].

[51] During the same deglaciation in which the Sahara Slide took place another large landslide, that

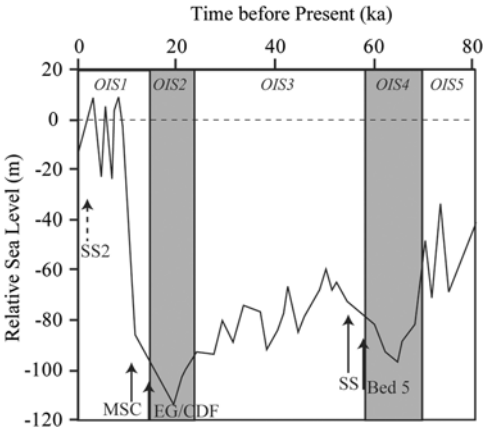

Figure 13. Timing of major mass slope failures on the African margin and the sea level curve from *Siddall et al.* [2003]. SS, Sahara Slide; EG/CDF, El Golfo/Canary Debris Flow; MSC, Mauritania Slide Complex; SS2, Sahara Slide reactivation. Oxygen isotope stages are indicated by white (interglacials) and gray shading (glacial). Note the apparent correlation between slide ages and periods of rising sea level.

gave rise to the Bed 5 deposit north of the Canary Islands, occurred on this margin [*Talling et al.*, 2007; *Wynn et al.*, 2002] (Figure 13). This suggests a major and regionally extensive event during that period. We therefore believe that climatic changes are a significant, if not the main, contributor to slope instability on the northwest African margin by controlling sedimentation rates, location of maximum accumulation rate and sea level and by consequence pore pressures. A link between sea level rise and landsliding is supported by the occurrence of the Mauritania Slide, further south on the NW African margin, during the rapid sea level rise at the Pleistocene/Holocene boundary (Figure 13) [*Wien et al.*, 2007].

[52] Repeated instability through geological time appears to be another common characteristic of slope areas on the NW African margin where Late Pleistocene landslides have been identified [*Antobreh and Krastel*, 2006; *Georgiopoulou et al.*, 2007]. This produces buried deposits of significant thickness and extent which would suggest that not only are slope failures a repetitive phenomenon on the northwest African margin but also when the slope fails it produces giant events.

6. Conclusions

[53] On the slope affected by the Sahara Slide, preferential weakening may have taken place due to sediment loading forcing pore fluids from sandy layers upward into the impermeable fine-grained slope sediments, leading to excess pore pressure buildup. Additional stress may have been induced by differential compaction of the underlying sediments that have filled the buried scar of an earlier landslide in the same location. Sea level change appears to be important but indirect in that it affects primary productivity and the locus of maximum sedimentation rate. Giant slides appear to coincide with periods of deglaciation, when the sedimentation rate was maximum and closer to shore.

[54] The Sahara Slide deposit is made up of at least two distinct units, suggesting more than one depositional event. Evidence points toward a retrogressive model of failure.

[55] Our analyses have revealed that a volcaniclastic turbidite deposited ~60 ka and originating from the nearby island of Hierro was eroded, entrained and mixed with the hemipelagic slope material of the slide at its base. The age of the Slide is therefore younger than the 60 ka old turbidite. We have also concluded that the slide was erosive, although the degree of erosion beneath the center of the flow is uncertain. The fact that the Sahara Slide is erosive suggests that hydroplaning was not the cause for the long runout distance. We suggest that excess pore pressure induced in the volcaniclastic sand (either by loading of the sand or by incorporation of water at the slide/seabed interface), and lubrication by the water-saturated seafloor sediments can explain the long runout of the slide. The lack of an associated turbidite deposit indicates that the slide mass did not disintegrate or mix significantly, probably as a result of (1) high cohesiveness of the failed fine-grained slope sediments, (2) relatively low flow velocities on gentle slopes, and (3) reduced basal friction once the flow started to run over the basal volcaniclastic sand layer. Slow slide flow velocities, low initial acceleration induced by the gentle gradient slopes and the retrogressive nature of the slide lead us to believe that the Sahara Slide was not tsunamigenic.

[56] Since the weak sediments related to the Sahara Slide have been evacuated from the scar area, and the probability of large earthquakes in the region is very low, it seems likely that the scar area is stable, at least in terms of landslides of dimensions similar to the Sahara Slide. However, the steep exposed headwall scarps have experienced recent instability, generating an extensive sediment gravity flow at 1–2 ka [*Georgiopoulou et al.*, 2009]. This has implications for other slides that are presently considered stable, even though they have similarly

steep headwalls exposed at the seafloor, e.g., the Storegga and Mauritania Slides [*Bryn et al.*, 2005; *Krastel et al.*, 2006].

[57] Major events on the northwest African margin appear coincident with glacial-to-interglacial transitions, i.e., periods of rising sea level. With imminent global warming and rising sea level [*Church and White*, 2006] further sliding on the northwest African margin as well as other passive margins perhaps might be anticipated.

Acknowledgments

[58] The authors would like to acknowledge the invaluable assistance of fellow cruise participants as well as the captains, officers, and crews of RRS *Charles Darwin* cruise 126 and R/V *Meteor* cruises 58/1 and 65/2. A. Georgiopoulou is thankful to the University of Southampton and the former Challenger Division of NOC for the provision of Ph.D. funding. The authors also wish to thank Sara Benetti, Peter Haughton, and Peter Talling for constructive discussions. The reviewers and editor of the journal are greatly appreciated for their invaluable comments.

References

Antobreh, A. A., and S. Krastel (2006), Morphology, seismic characteristics and development of Cap Timiris Canyon, offshore Mauritania: A newly discovered canyon preserved-off a major and climatic region, *Mar. Pet. Geol.*, *23*(1), 37–59, doi:10.1016/j.marpetgeo.2005.06.003.

Bardet, J.-P., C. E. Synolakis, H. L. Davies, F. Imamura, and E. A. Okal (2003), Landslide tsunamis: Recent findings and research directions, *Pure Appl. Geophys.*, *160*, 1793–1809, doi:10.1007/s00024-003-2406-0.

Bertrand, P., et al. (1996), The glacial ocean productivity hypothesis: The importance of regional temporal and spatial studies, *Mar. Geol.*, *130*, 1–9, doi:10.1016/0025-3227(95)00166-2.

Bozzano, G., H. Kuhlmann, and B. Alonso (2002), Storminess control over African dust input to the Moroccan Atlantic margin (NW Africa) at the time of maxima boreal summer insolation: A record of the last 220 kyr, *Palaeogeogr. Palaeoclimatol. Palaeoecol.*, *183*(1–2), 155–168, doi:10.1016/S0031-0182(01)00466-7.

Bryn, P., A. Solheim, K. Berg, R. Lien, C. F. Forsberg, H. Haflidason, D. Ottesen, and L. Rise (2003), The Storegga Slide complex: Repeated large scale sliding in response to climatic cyclicity, in *Submarine Mass Movements and Their Consequences*, edited by J. Locat and J. Mienert, pp. 215–222, Kluwer Acad., Dordrecht, Netherlands.

Bryn, P., K. Berg, C. F. Forsberg, A. Solheim, and T. J. Kvalstad (2005), Explaining the Storegga Slide, *Mar. Pet. Geol.*, *22*, 11–19, doi:10.1016/j.marpetgeo.2004.12.003.

Church, J. A., and N. J. White (2006), A 20th century acceleration in global sea-level rise, *Geophys. Res. Lett.*, *33*, L01602, doi:10.1029/2005GL024826.

Dutta, N. C. (1984), Shale compaction and abnormal pore pressure: A model of geopressure in the Gulf Coast basin, *Geophysics*, *49*, 660.

Embley, R. W. (1976), New evidence for occurrence of debris flow deposits in the deep sea, *Geology*, *4*, 371–374, doi:10.1130/0091-7613(1976)4<371:NEFOOD>2.0.CO;2.

Embley, R. W. (1980), The role of mass transport in the distribution and character of deep-ocean sediments in the Atlantic, *Mar. Geol.*, *38*, 23–50, doi:10.1016/0025-3227(80)90050-X.

Embley, R. W. (1982), Anatomy of some Atlantic margin sediment slides and some comments on ages and mechanisms, in *Marine Slides and Other Mass Movements*, edited by S. Saxov and J. K. Neiuwenhuis, pp. 189–214, Plenum, New York.

Embley, R. W., and R. D. Jacobi (1977), Distribution and morphology of large submarine slides and slumps on Atlantic continental margins, *Mar. Geotechnol.*, *2*, 205–228, doi:10.1080/10641197709379780.

Flemings, P.B., H. Long, B. Dugan, J. Germain, C.M. John, J.H. Behrmann, D. Sawyer, and IODP Expedition 308 Scientists (2008), Pore pressure penetrometers document high overpressure near the seafloor where multiple submarine landslides have occurred on the continental slope, offshore Louisiana, Gulf of Mexico, *Earth Planet. Sci. Lett.*, *269*(3–4), 309–332. (Erratum, *Earth Planet. Sci. Lett.*, *274*, 269–283, doi:10.1016/j.epsl.2008.06.027, 2008.)

Frenz, M., R. B. Wynn, A. Georgiopoulou, V. B. Bender, G. Hough, D. G. Masson, P. J. Talling, and B. T. Cronin (2009), Provenance and pathways of late Quaternary turbidites in the deep-water Agadir Basin, northwest African margin, *Int. J. Earth Sci.*, *98*(4), 721–733, doi:10.1007/s00531-008-0313-4.

Gee, M. J. R., D. G. Masson, A. B. Watts, and P. A. Allen (1999), The Saharan debris flow: An insight into the mechanics of long runout submarine debris flows, *Sedimentology*, *46*, 317–335, doi:10.1046/j.1365-3091.1999.00215.x.

Gee, M. J. R., D. G. Masson, A. B. Watts, and N. C. Mitchell (2001), Passage of debris flows and turbidity currents through a topographic constriction: Seafloor erosion and deflection of pathways, *Sedimentology*, *48*, 1389–1409, doi:10.1046/j.1365-3091.2001.00427.x.

Georgiopoulou, A., S. Krastel, D. G. Masson, and R. B. Wynn (2007), Repeated instability of the NW African margin related to buried landslide scarps, in *Submarine Mass Movements and Their Consequences*, edited by V. Lykousis, D. Sakellariou, and J. Locat, pp. 29–36, Springer, Dordrecht, Netherlands.

Georgiopoulou, A., R. B. Wynn, D. G. Masson, and M. Frenz (2009), Linked turbidite-debrite resulting from recent Sahara Slide headwall reactivation, *Mar. Pet. Geol.*, *26*(10), 2021–2031, doi:10.1016/j.marpetgeo.2009.02.013.

Haflidason, H., H. P. Sejrup, A. Nygård, J. Mienert, P. Bryn, L. Lien, C. F. Forsberg, K. Berg, and D. G. Masson (2004), The Storegga Slide: Architecture, geometry and slide development, *Mar. Geol.*, *213*(1–4), 201–234, doi:10.1016/j.margeo.2004.10.007.

Haflidason, H., R. Lien, H. P. Sejrup, C. F. Forsberg, and P. Bryn (2005), The dating and morphometry of the Storegga Slide, *Mar. Pet. Geol.*, *22*, 123–136, doi:10.1016/j.marpetgeo.2004.10.008.

Harbitz, C.B., G. Parker, A. Elverhoi, J.G. Marr, D. Mohrig, and P.A. Harff (2003), Hydroplaning of subaqueous debris flows and glide blocks: Analytical solutions and discussion, *J. Geophys. Res.*, *108*(B7), 2349, doi:10.1029/2001JB001454.

Harbitz, C. B., F. Løvholt, G. Pedersen, and D. G. Masson (2006), Mechanisms of tsunami generation by submarine landslides: A short review, *Norw. J. Geol.*, *86*(3), 255–264.

Haugen, K. B., F. Lovholt, and C. B. Harbitz (2005), Fundamental mechanisms for tsunami generation by submarine mass flows in idealised geometries, *Mar. Pet. Geol.*, *22*(1–2), 209–217, doi:10.1016/j.marpetgeo.2004.10.016.

Haughton, P. D. W., S. P. Barker, and W. D. McCaffrey (2003), 'Linked' debrites in sand-rich turbidite systems–origin and significance, *Sedimentology*, *50*(3), 459–482.

Hayes, D. E., and P. D. Rabinowitz (1975), Mesozoic magnetic lineations and the magnetic quiet zone off northwest Africa, *Earth Planet. Sci. Lett.*, *28*, 105–115, doi:10.1016/0012-821X(75)90217-4.

Henrich, R., T. J. J. Hanebuth, S. Krastel, N. Neubert, and R. B. Wynn (2008), Architecture and sediment dynamics of the Mauritania Slide Complex, *Mar. Pet. Geol.*, *25*, 17–33, doi:10.1016/j.marpetgeo.2007.05.008.

Huehnerbach, V., D. G. Masson, and Partners of the COSTA-Project (2004), Landslides in the North Atlantic and its adjacent seas: An analysis of their morphology, setting and behaviour, *Mar. Geol.*, *213*(1–4), 343–362, doi:10.1016/j.margeo.2004.10.013.

Krastel, S., R. B. Wynn, T. Hanebuth, R. Henrich, C. Holz, H. Meggers, H. Kuhlman, A. Georgiopoulou, and H. Schulz (2006), Mapping of seabed morphology and shallow sediment structure of the Mauritania continental margin, North Africa: Some implications on the geohazard potential, *Norw. J. Geol.*, *86*, 163–176.

Kuhlmann, H., T. Freudenthal, P. Helmke, and H. Meggers (2004), Reconstruction of paleoceanography off NW Africa during the last 40,000 years: Influence of local and regional factors on sediment accumulation, *Mar. Geol.*, *207*, 209–224, doi:10.1016/j.margeo.2004.03.017.

Kvalstad, T. J., L. Andresen, C. F. Forsberg, K. Berg, P. Bryn, and M. Wangen (2005), The Storegga slide: Evaluation of triggering sources and sliding mechanics, *Mar. Pet. Geol.*, *22*, 245–256, doi:10.1016/j.marpetgeo.2004.10.019.

Loncke, L., et al. (2009), Multi-scale slope instabilities along the Nile deep-sea fan, Egyptian margin: A general overview, *Mar. Pet. Geol.*, *26*(5), 633–646, doi:10.1016/j.marpetgeo.2008.03.010.

Masson, D. G., R. B. Kidd, J. V. Gardner, Q. J. Huggett, and P. P. E. Weaver (1992). Saharan continental rise: Facies distribution and sediment slides, in *Geologic Evolution of the Atlantic Continental Rise*, edited by C. W. Poag and P. C. deGraciansky, pp. 327–343, Van Nostrand Reinhold, New York.

Masson, D. G., Q. J. Huggett, and D. Brunsden (1993), The surface texture of the Saharan Debris Flow deposit and some speculations on submarine debris flow processes, *Sedimentology*, *40*(3), 583–598, doi:10.1111/j.1365-3091.1993.tb01351.x.

Masson, D. G., B. van Niel, and P. P. E. Weaver (1997), Flow processes and sediment deformation in the Canary Debris Flow on the NW African Continental Rise, *Sediment. Geol.*, *110*, 163–179, doi:10.1016/S0037-0738(96)00089-9.

Masson, D. G., M. Canals, B. Alonso, R. Urgeles, and V. Huehnerbach (1998), The Canary Debris Flow: Source area morphology and failure mechanisms, *Sedimentology*, *45*, 411–432, doi:10.1046/j.1365-3091.1998.0165f.x.

Masson, D. G., R. B. Wynn, and P. J. Talling (2009), Large landslides on passive continental margins: Processes, hypotheses and outstanding questions, in *Submarine Mass Movements and Their Consequences*, edited by D. C. Mosher et al., pp. 153–165, Springer, Dordrecht, Netherlands.

McAdoo, B. G., L. F. Pratson, and D. Orange (2000), Submarine landslide geomorphology, US continental margin, *Mar. Geol.*, *169*, 103–136, doi:10.1016/S0025-3227(00)00050-5.

Mohrig, D., K. X. Whipple, M. Hondzo, C. Ellis, and G. Parker (1998), Hydroplaning of subaqueous debris flows, *Geol. Soc. Am. Bull.*, *110*(3), 387–394, doi:10.1130/0016-7606(1998)110<0387:HOSDF>2.3.CO;2.

Mohrig, D., A. Elverhoi, and G. Parker (1999), Experiments on the relative mobility of muddy subaqueous and subaerial debris flows, and their capacity to remobilize antecedent deposits, *Mar. Geol.*, *154*, 117–129, doi:10.1016/S0025-3227(98)00107-8.

Moreno, A., J. Targarona, J. Henderiks, M. Canals, T. Freudenthal, and H. Meggers (2001), Orbital forcing of dust supply to the North Canary Basin over the last 250 kyr, *Quat. Sci. Rev.*, *20*, 1327–1339, doi:10.1016/S0277-3791(00)00184-0.

Piper, D. J. W., P. Cochonat, and M. Morrison (1999), The sequence of events around the epicentre of the 1929 Grand Banks earthquake: Initiation of debris flows and turbidity current inferred from sidescan sonar, *Sedimentology*, *46*, 79–97, doi:10.1046/j.1365-3091.1999.00204.x.

Sarnthein, M., U. Pflaumann, R. Ross, R. Tiedemann, and K. Winn (1992), Transfer functions to reconstruct ocean palaeoproductivity: A comparison, in *Upwelling Systems: Evolution Since the Early Miocene*, edited by C. P. Summerhayes, W. L. Prell, and K. C. Emeis, *Geol. Soc. Spec. Publ.*, *64*, 411–427.

Siddall, M., E. J. Rohling, A. Almogi-Labin, C. Hemleben, D. Meischner, I. Schmelzer, and D. A. Smeed (2003), Sea-level fluctuations during the last glacial cycle, *Nature*, *423*(6942), 853–858, doi:10.1038/nature01690.

Simm, R. W., and R. B. Kidd (1984), Submarine debris flow deposits detected by long-range side-scan sonar 1.000-kilometers from source, *Geo Mar. Lett.*, *3*, 13–16, doi:10.1007/BF02463436.

Strout, J. M., and T. I. Tjelta (2005), In situ pore pressures: What is their significance and how can they be reliably measured?, *Mar. Pet. Geol.*, *22*, 275–285, doi:10.1016/j.marpetgeo.2004.10.024.

Summerhayes, C. P., J. D. Milliman, S. R. Briggs, A. G. Bee, and C. Hogan (1976), Northwest African shelf sediments: Influence of climate and sedimentary processes, *J. Geol.*, *84*, 277–300, doi:10.1086/628196.

Talling, P. J., et al. (2007), Onset of submarine debris flow deposition far from original giant landslide, *Nature*, *450*(7169), 541–544, doi:10.1038/nature06313.

ten Brink, U. S., H. J. Lee, E. L. Geist, and D. Twichell (2009), Assessment of tsunami hazard to the U.S. East Coast using relationships between submarine landslides and earthquakes, *Mar. Geol.*, *264*(1–2), 65–73, doi:10.1016/j.margeo.2008.05.011.

Toniolo, H., P. Harff, J. Marr, C. Paola, and G. Parker (2004), Experiments on reworking by successive unconfined subaqueous and subaerial muddy debris flows, *J. Hydraul. Eng.*, *130*(1), 38–48, doi:10.1061/(ASCE)0733-9429(2004)130:1(38).

Twichell, D. C., J. D. Chaytor, U. S. ten Brink, and B. Buczkowski (2009), Morphology of late Quaternary submarine landslides along the U.S. Atlantic continental margin, *Mar. Geol.*, *264*(1–2), 4–15, doi:10.1016/j.margeo.2009. 01.009.

Vendeville, B. C., and V. Gaullier (2003), Role of pore-fluid pressure and slope angle in triggering submarine mass movements: Natural examples and pilot experimental models, in

Submarine Mass Movements and Their Consequences, edited by J. Locat and J. Mienert, pp. 137–144, Kluwer Acad., Dordrecht, Netherlands.

Ward, S. N. (2001), Landslide tsunami, *J. Geophys. Res.*, *106*(B6), 11,201–11,215, doi:10.1029/2000JB900450.

Watts, P., S. T. Grilli, D. R. Tappin, and G. J. Fryer (2005), Tsunami generation by submarine mass failure. II: Predictive equations and case studies, *J. Waterw. Port Coastal Ocean Eng.*, *131*(6), 298–310, doi:10.1061/(ASCE)0733-950X(2005)131:6(298).

Weaver, P. P. E., and A. Kuijpers (1983), Climatic control of turbidite deposition on the Madeira Abyssal Plain, *Nature*, *306*, 360–363, doi:10.1038/306360a0.

Weaver, P. P. E., and J. Thomson (1993), Calculating erosion by deep-sea turbidity currents during initiation and flow, *Nature*, *364*, 136–138, doi:10.1038/364136a0.

Weaver, P. P. E., R. B. Wynn, N. H. Kenyon, and J. Evans (2000), Continental margin sedimentation, with special reference to the north-east Atlantic margin, *Sedimentology*, *47*, suppl. 1, 239–256, doi:10.1046/j.1365-3091.2000.0470s1239.x.

Wien, K., C. Holz, M. Kolling, and H. D. Schulz (2006), Age models for pelagites and turbidites from the Cap Timiris Canyon off Mauritania, *Mar. Pet. Geol.*, *23*(3), 337–352, doi:10.1016/j.marpetgeo.2005.10.005.

Wien, K., M. Kölling, and H. D. Schulz (2007), Age models for the Cape Blanc Debris Flow and the Mauritania Slide Complex in the Atlantic Ocean off NW Africa, *Quat. Sci. Rev.*, *26*(19–21), 2558–2573, doi:10.1016/j.quascirev.2007.06.018.

Wynn, R. B., P. P. E. Weaver, D. G. Masson, and D. A. V. Stow (2002), Turbidite depositional architecture across three interconnected deep-water basins on the north-west African margin, *Sedimentology*, *49*, 669–695, doi:10.1046/j.1365-3091.2002.00471.x.